Supporting Information

Photopolymerized helical acrylate networks enable stable and full-color circularly polarized luminescence in perovskite nanocrystals

Atanu Jana*, Deblina Das, Sourav Mal, Tarak Nath Mandal, Youngsin Park*, and Sangeun Cho*

A. Jana, D. Das, S. Mal, S. Cho

Division of System Semiconductor, Dongguk University, Seoul 04620, Republic of Korea.

T. N. Mandal

Department of Chemistry, SRM Institute of Science and Technology, Kattankulathur, Tamil Nadu 603203, India.

Y. Park

Department of Chemistry, College of Natural Science, Ulsan National Institute of Science and Technology, Ulsan 44919, Republic of Korea.

Synthesis of pristine $CsPbX_3$ (X = Cl/Br/I) NCs

Synthesis of $CsPbCl_3$ NCs

To synthesize cesium oleate, 0.814 g of Cs_2CO_3 was placed in a 100 mL two-neck flask along with 40 mL of octadecene (ODE, 90%, Sigma-Aldrich) and 2.5 mL of OA. The mixture was first dried under vacuum at 120 °C for 1 hour to remove moisture and volatile impurities. It was then heated under a nitrogen atmosphere to 150 °C, allowing Cs_2CO_3 to fully react with oleic acid to form cesium oleate. Because cesium oleate tends to precipitate out of ODE at room temperature, the prepared solution must be preheated to 100 °C prior to use or injection in subsequent synthesis steps.

To prepare $CsPbCl_3$ NCs, 5 mL of octadecene (ODE), 1 mL of trioctylphosphine (TOP), and 0.057 g (0.2 mmol) of lead (II) chloride ($PbCl_2$) were added to a 25 mL two-neck flask and dried under vacuum at 150 °C for 1 hour. Following the drying step, 0.5 mL of pre-dried oleylamine (OLA, 90%, Sigma-Aldrich) and 0.5 mL of pre-dried oleic acid (OA, 90%, Sigma-Aldrich) were injected into the flask under a nitrogen atmosphere at 150 °C. Once $PbCl_2$ had completely dissolved (within approximately 10 minutes), the reaction temperature was increased to 180 °C. At this stage, 0.4 mL of preheated Cs-oleate solution (0.125 M in ODE, prepared as previously described) was swiftly injected. After 15 seconds, the reaction was rapidly quenched using an ice-water bath. To isolate the $CsPbCl_3$ NCs, the crude reaction mixture was centrifuged at 10,000 rpm for 10 minutes, and the supernatant was discarded. The resulting nanocrystal pellet was then redispersed in toluene for further applications.

Synthesis of $CsPbBr_3$ NCs

In a 25 mL two-neck flask, 5 mL of ODE and 0.073 g (0.2 mmol) of $PbBr_2$ were combined and dried under vacuum at 120 °C for 1 hour to remove residual moisture. Once dried, 0.5 mL of

OLA and 0.5 mL of OA, both pre-dried, were added to the flask under a nitrogen atmosphere at 120 °C. After the $PbBr_2$ had fully dissolved (within approximately 10 minutes), the mixture was heated to 150 °C. At this point, 0.4 mL of preheated Cs-oleate solution (0.125 M in ODE) was swiftly injected. Exactly 15 seconds after the injection, the reaction was rapidly quenched by immersing the flask in an ice-water bath. To isolate the $CsPbBr_3$ NCs, the crude product was centrifuged at 10,000 rpm for 10 minutes, and the supernatant was discarded. The resulting pellet, containing the NCs, was redispersed in toluene for further processing or characterization.

Synthesis of $CsPbI_3$ NCs

In a 25 mL two-neck flask, 5 mL of octadecene (ODE) and 0.092 g (0.2 mmol) of lead(II) iodide (PbI_2) were combined and dried under vacuum at 180 °C for 1 hour to remove moisture and volatiles. Once dried, 0.5 mL each of pre-dried oleylamine (OLA, 90%, Sigma-Aldrich) and oleic acid (OA, 90%, Sigma-Aldrich) were injected into the flask at 150 °C under a nitrogen atmosphere. After complete dissolution of PbI_2 (typically within 10 minutes), the temperature was increased to 180 °C, and 0.4 mL of preheated Cs-oleate solution (0.125 M in ODE, prepared as previously described) was rapidly injected. After 15 seconds, the reaction mixture was promptly cooled using an ice-water bath to halt further growth. To isolate the $CsPbI_3$ NCs, the crude product was centrifuged at 10,000 rpm for 10 minutes, and the supernatant was discarded. The resulting nanocrystal pellet was redispersed in toluene for further characterization or use.

In-situ synthesis process $CsPbBr_3$ NCs@DPAHA in ethanol:

The branched polymer, DPAHA was prepared through a UV-induced photopolymerization process using DPEPA/HEA as the monomer. Initially, 0.1 g of the monomer was dissolved in 2 mL of ethanol, 5 mg $CsPbBr_3$, and 20 μL of HMPP was added as the photoinitiator. This mixture was then exposed to ultraviolet light and monitored at 45-minute intervals.

In-situ synthesis process $CsPbBr_3$ NCs@DPAHA in toluene:

The branched polymer, DPAHA was prepared through a UV-induced photopolymerization process using DPEPA/HEA as the monomer. Initially, 0.1 g of the monomer was dissolved in 2 mL of toluene, 5 mg $CsPbBr_3$, and 20 μL of HMPP was added as the photoinitiator. This mixture was then exposed to ultraviolet light and monitored at 45-minute intervals.

Figures

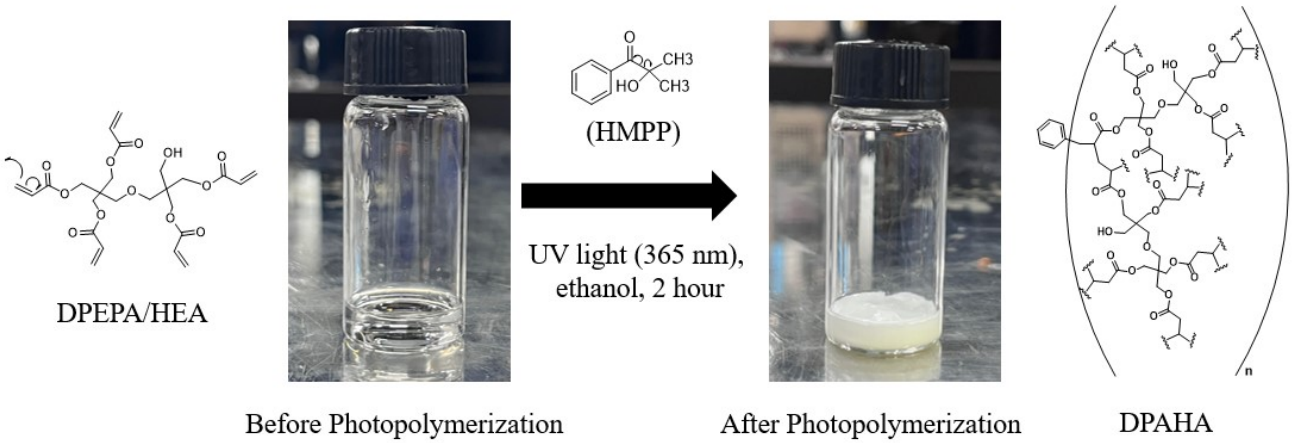

Fig. S1. Synthesis of DPAHA via photopolymerization reaction using HMMP was added as the photoinitiator. The branched polymer DPAHA was synthesized via photoinitiated crosslinking polymerization of DPEPA/HEA. Upon UV irradiation, the photoinitiator HMPP undergoes Norrish type I α-cleavage to generate benzoyl and tert-butyl radicals. The benzoyl radicals initiate free radical polymerization of the acrylate monomers, propagating chain growth and branching. Continued reaction of residual vinyl groups leads to a three-dimensional crosslinked polymer network.

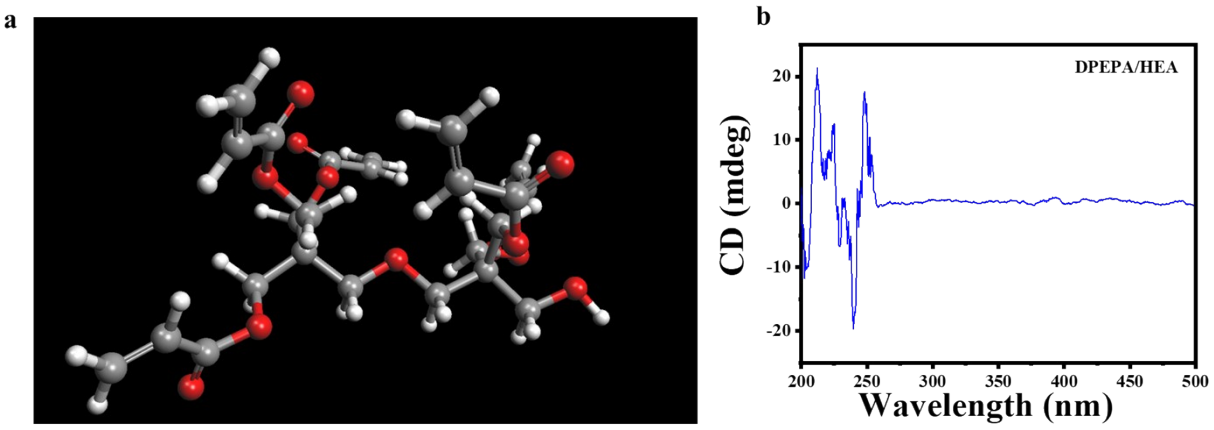

Fig. S2. (a) Schematic three-dimensional representation of DPEPA/HEA. (b) CD spectrum. DPEPA/HEA does not contain any tetrahedral chiral center, yet its flexible branched structure induces a non-planar, asymmetrical conformation that lacks symmetry elements, allowing the molecule to become chiral and thereby produce a measurable circular dichroism (CD) signal.

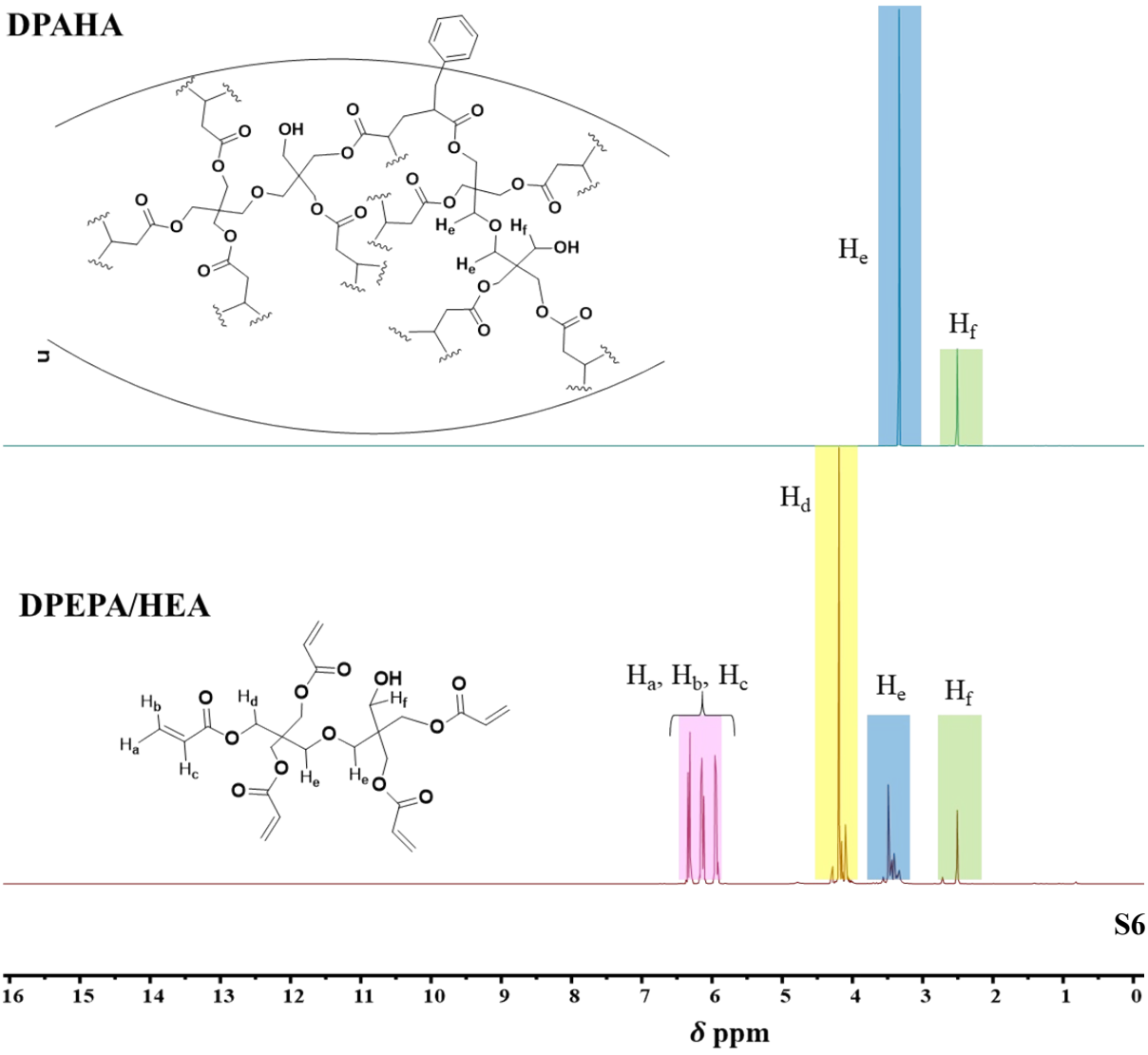

Fig. S3. Solid-state ^{1}H-NMR spectrum DPEPA/HEA monomer (bottom) and DPAHA polymer (top).

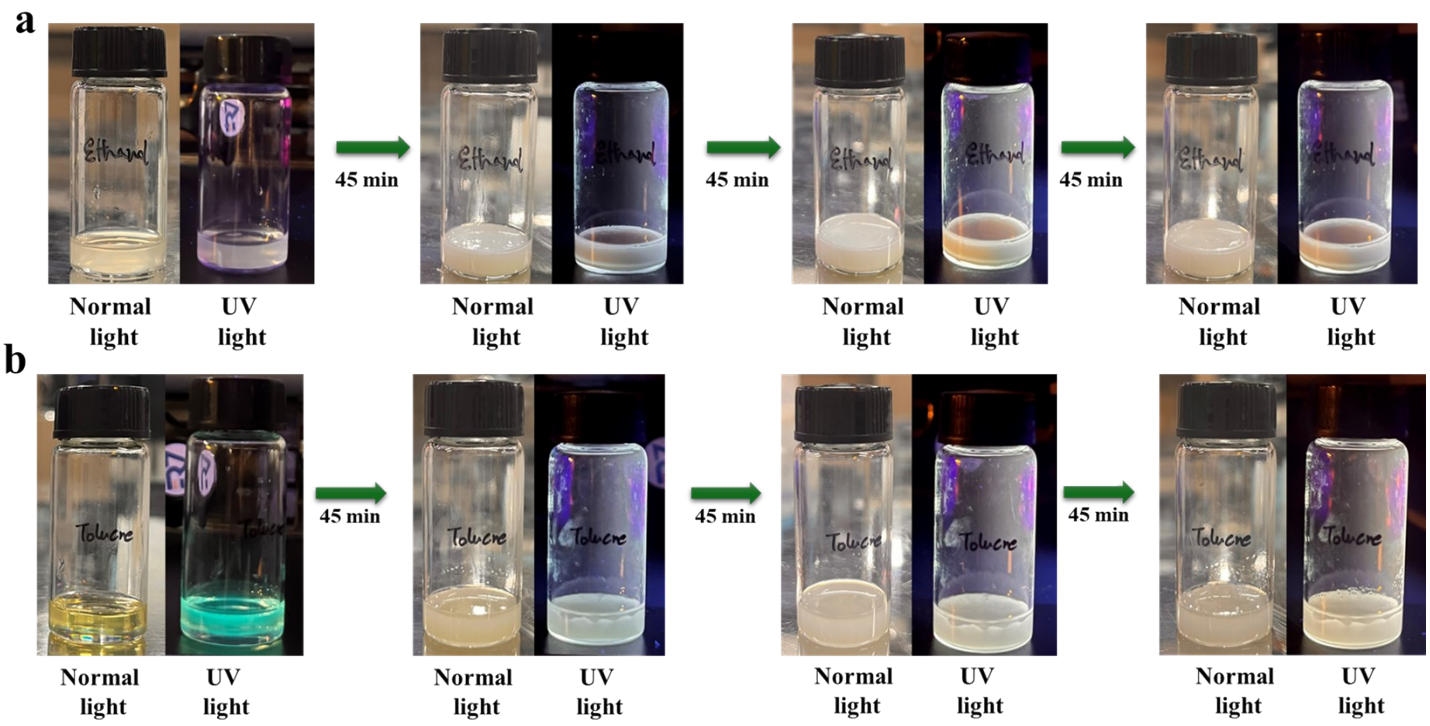

Fig. S4. In-situ polymerization reaction to encapsulate $CsPbBr_3$ NCs inside DPAHA: (a) etheanol (b) toluene. In both the cases, $CsPbBr_3$ NCs lose its photoluminescence properties.

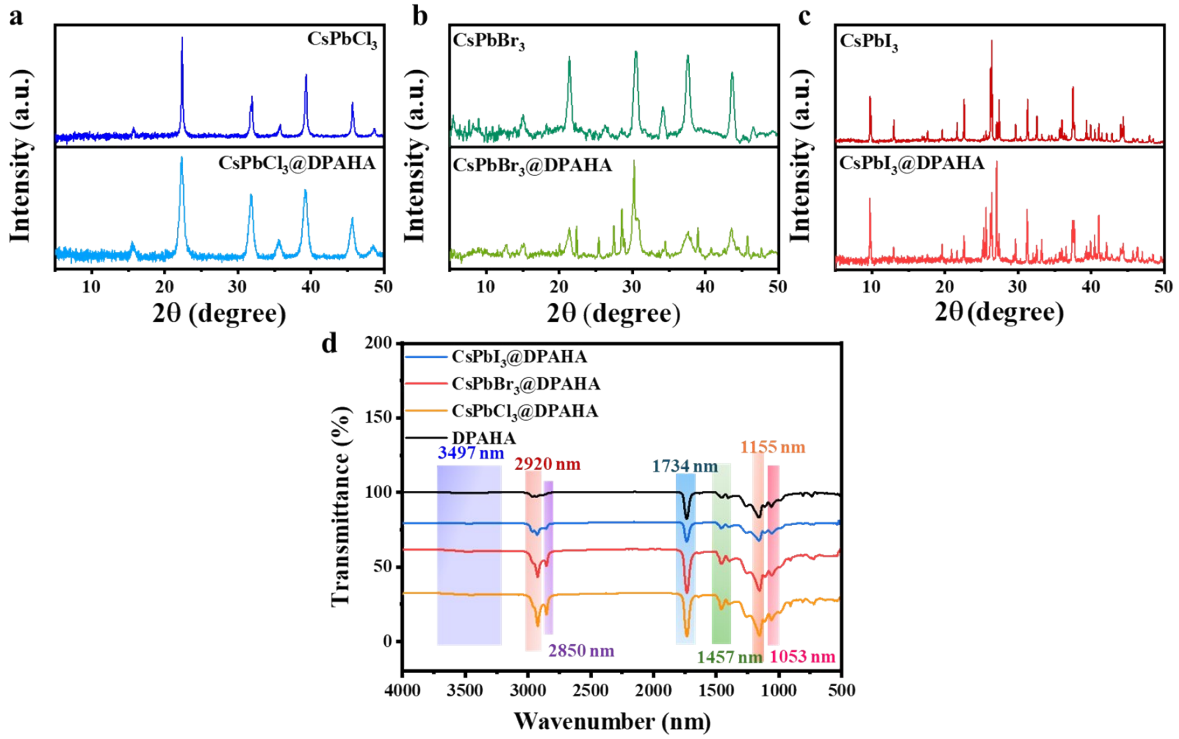

Fig. S5: **a.** XPD spectrum of pure $CsPbCl_3$ and $CsPbCl_3$@DPAHA; **b.** XPD spectrum of pure $CsPbBr_3$ and $CsPbBr_3$@DPAHA; **c.** XPD spectrum of pure $CsPbI_3$ and $CsPbI_3$@DPAHA; **d.** FTIR spectrum of DPAHA and $CsPbX_3$@DPAHA

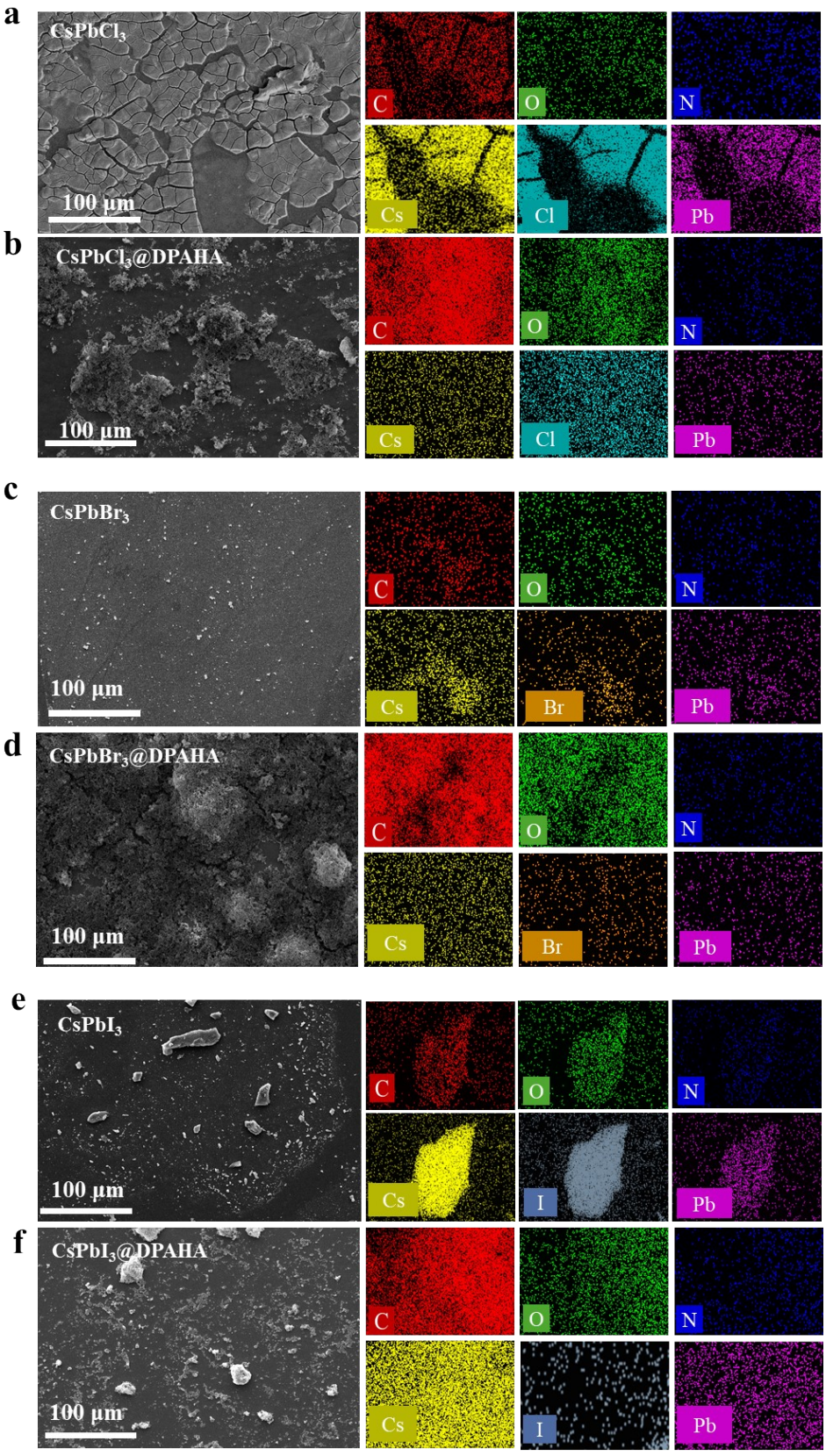

Fig. S6. SEM image and EDS mapping of a) pristine $CsPbCl_3$; b) $CsPbCl_3$@DPAHA. c) pristine $CsPbBr_3$; and d) $CsPbBr_3$@DPAHA, e) pristine $CsPbI_3$; f) $CsPbI_3$@DPAHA

a

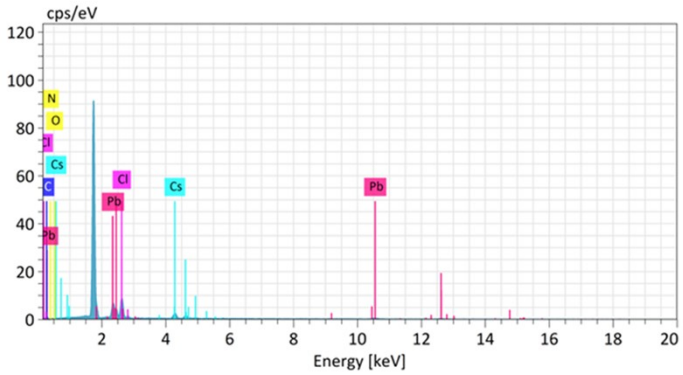

b

Element	At. No.	Net	Mass [%]	Mass Norm. [%]	Atom [%]	abs. error [mass%] (3σ)
C	6	1073	12.19	16.92	56.34	2.41
N	7	104	1.59	2.21	6.31	0.80
O	8	263	1.84	2.56	6.40	0.64
Cs	55	7818	13.45	18.66	5.62	1.51
Pb	82	2090	32.26	44.89	8.67	5.93
Cl	17	14092	10.65	14.77	16.67	1.20
		Sum	**72.09**	**100.00**	**100.00**	

c

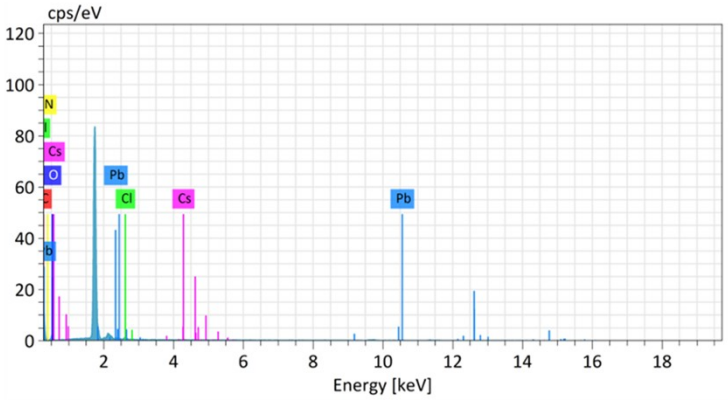

d

Element	At. No.	Net	Mass [%]	Mass Norm. [%]	Atom [%]	abs. error [mass%] (3σ)
C	6	12702	22.32	65.99	76.02	10.01
N	7	55	2.12	1.78	1.76	1.52
O	8	2332	3.53	24.35	21.06	4.24
Cs	55	650	9.41	1.84	0.19	0.56
Pb	82	167	21.22	4.26	0.28	2.72
Cl	17	1519	8.34	1.79	0.70	1.52
		Sum	**66.94**	**100.00**	**100.00**	

Fig. S7: SEM-EDS spectra and elemental composition. a. pure $CsPbCl_3$ and **b.** $CsPbCl_3$@DPAHA

a

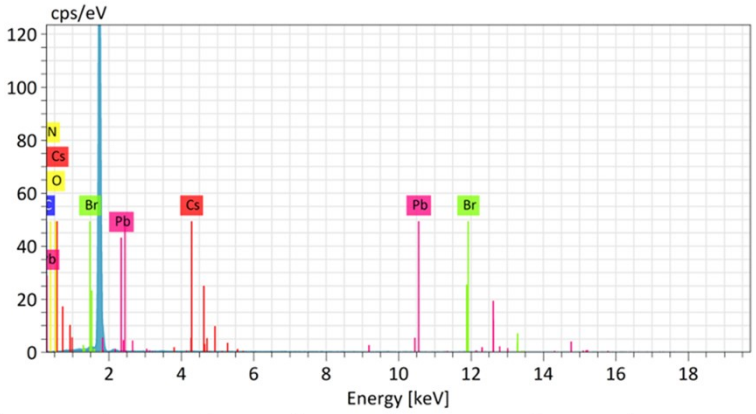

b

Element	At. No.	Net	Mass [%]	Mass Norm. [%]	Atom [%]	abs. error [mass%] (3σ)
C	6	114	2.05	23.72	61.49	2.31
N	7	0.00	0.00	0.00	0.00	0.00
O	8	80	0.80	9.31	18.11	0.65
Cs	55	428	0.91	10.51	2.46	0.45
Pb	82	67	1.47	17.01	2.56	1.38
Br	35	115	3.41	39.46	15.38	2.47
		Sum	**8.68**	**100.00**	**100.00**	

c

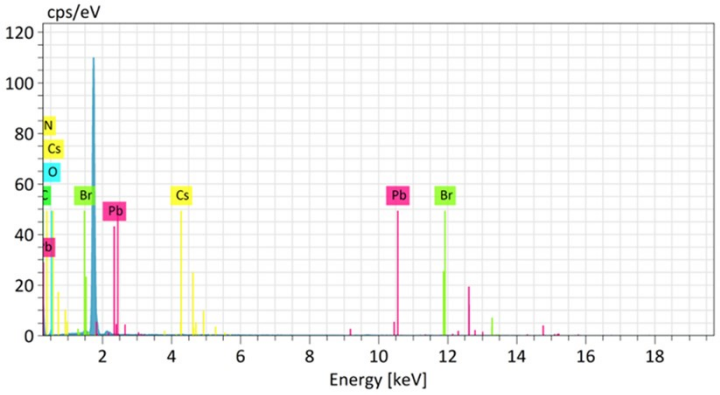

d

Element	At. No.	Net	Mass [%]	Mass Norm. [%]	Atom [%]	abs. error [mass%] (3σ)
C	6	13308	24.13	70.33	80.80	10.69
N	7	0.00	0.00	0.00	0.00	0.00
O	8	1984	2.84	20.97	18.08	3.76
Cs	55	786	10.03	1.96	0.20	0.52
Pb	82	102	18.83	2.37	0.16	1.50
Br	35	138	3.38	4.37	0.75	2.37
		Sum	**59.21**	**100.00**	**100.00**	

Fig. S8: SEM-EDS spectra and elemental composition. a. pure $CsPbBr_3$ and **b.** $CsPbBr_3$@DPAHA

a

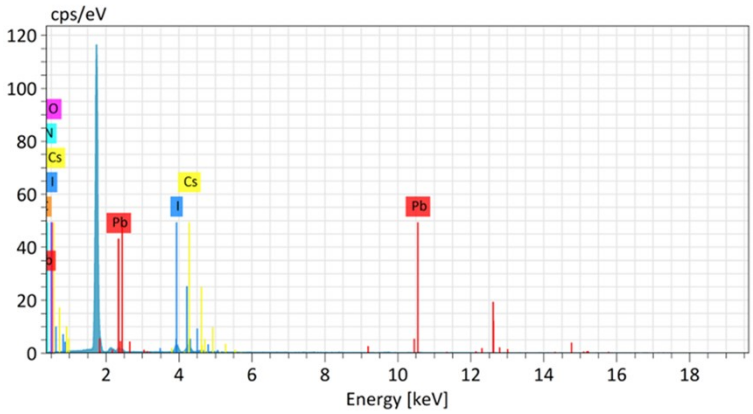

b

Element	At. No.	Net	Mass [%]	Mass Norm. [%]	Atom [%]	abs. error [mass%] (3σ)
C	6	400	2.91	7.95	47.51	0.81
N	7	213	0.73	1.02	1.98	0.23
O	8	104	0.50	1.36	6.12	0.41
Cs	55	4565	9.00	23.54	11.29	1.19
Pb	82	430	7.20	19.65	6.81	2.51
I	53	9269	17.02	46.47	26.29	1.90
		Sum	**37.36**	**100.00**	**100.00**	

c

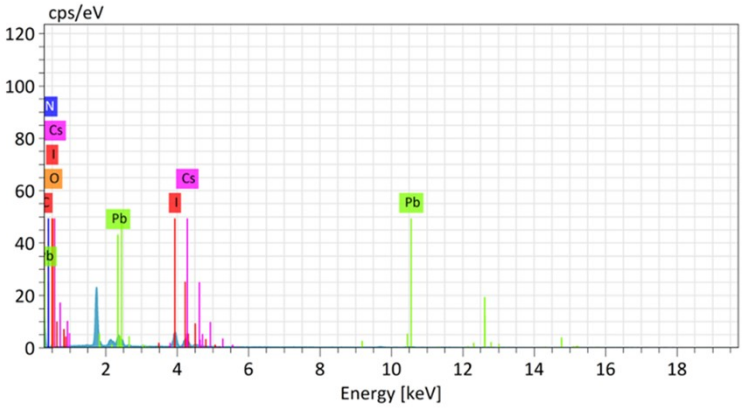

d

Element	At. No.	Net	Mass [%]	Mass Norm. [%]	Atom [%]	abs. error [mass%] (3σ)
C	6	18130	26.76	40.00	79.48	4.13
N	7	278	1.31	1.96	3.34	0.42
O	8	2071	3.89	5.81	8.67	0.69
Cs	55	6847	4.90	7.32	1.31	0.57
Pb	82	1535	11.48	17.17	1.98	2.19
I	53	288812	18.56	27.74	5.22	1.55
		Sum	**66.90**	**100.00**	**100.00**	

Fig. S9: SEM-EDS spectra and elemental composition. a. pure $CsPbI_3$ and **b.** $CsPbI_3$@DPAHA

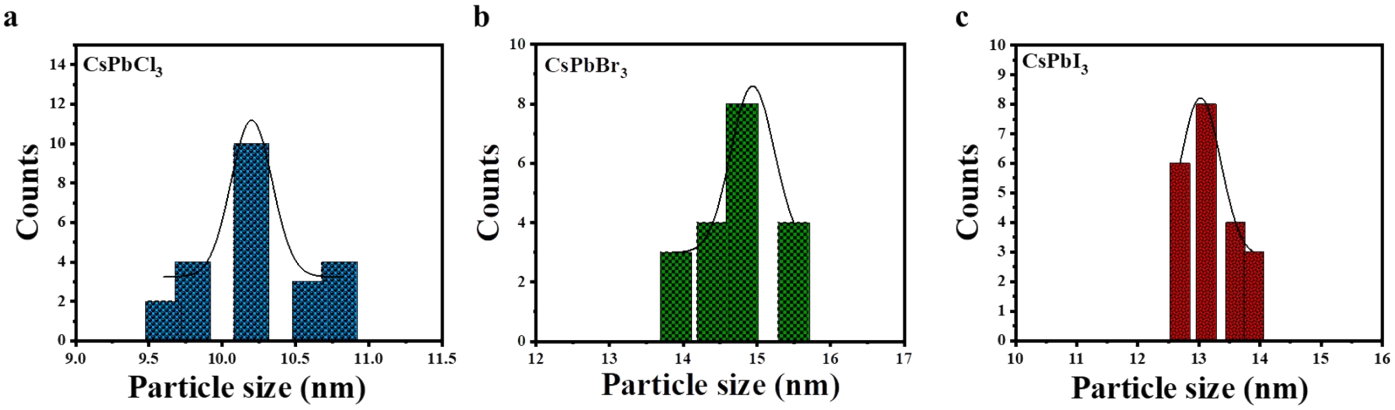

Fig. S10: Particle size distribution histograms (a) $CsPbCl_3$, (b) $CsPbBr_3$ NCs, (c) $CsPbI_3$ NCs.

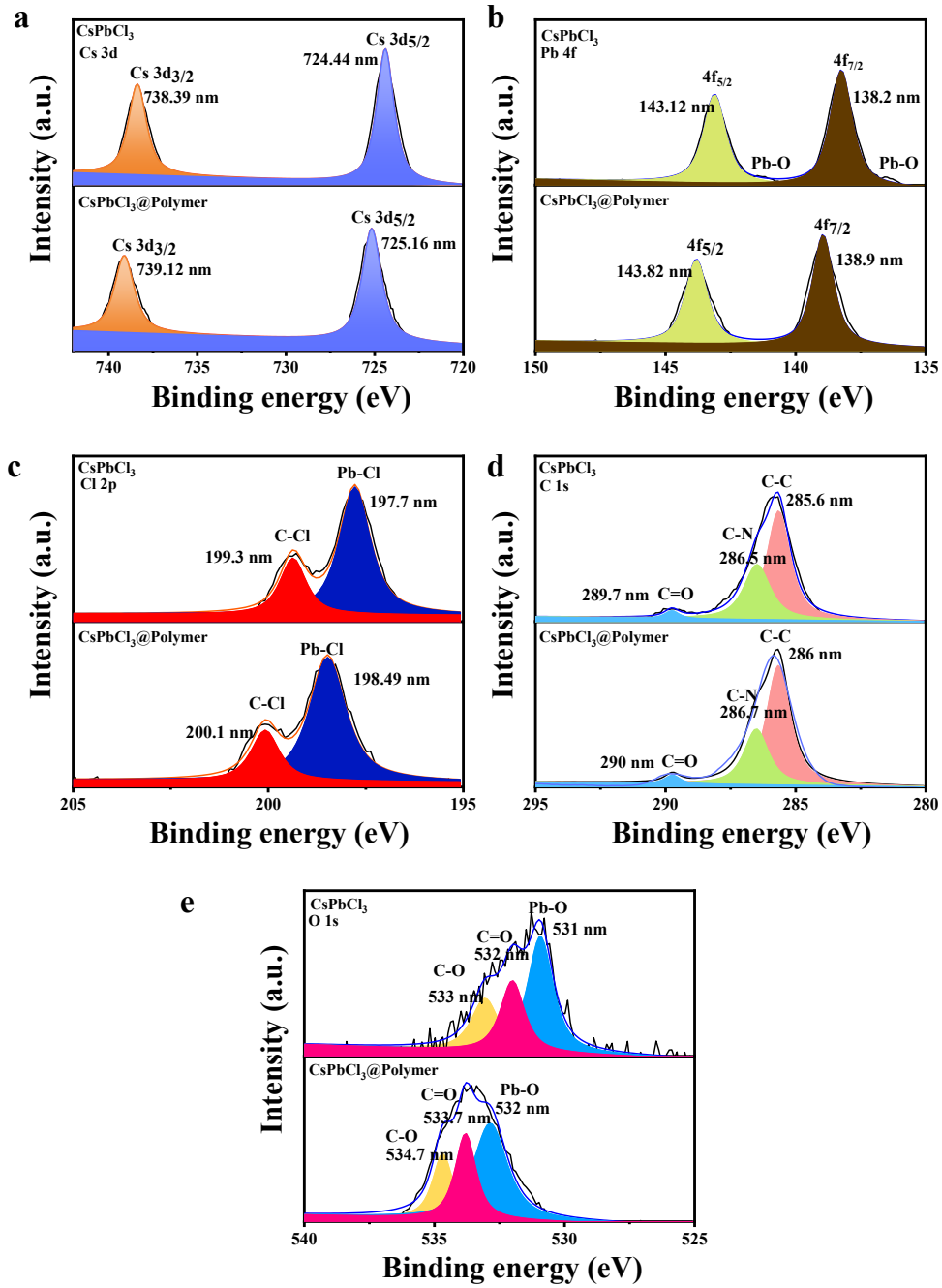

Fig. S11: **a.** XPS spectrum of Cs 3d of pure $CsPbCl_3$ and $CsPbCl_3$@DPAHA; **b.** XPS spectrum of Pb 4f of pure $CsPbCl_3$ and $CsPbCl_3$@DPAHA; **c.** XPS spectrum of Cl 2p of pure $CsPbCl_3$ and $CsPbCl_3$@DPAHA; **d.** XPS spectrum of C 1s of pure $CsPbCl_3$ and $CsPbCl_3$@DPAHA; **e**. XPS spectrum of O 1s of pure $CsPbCl_3$ and $CsPbCl_3$@DPAHA.

XPS was used to investigate the surface chemistry of $CsPbCl_3$ NCs and $CsPbCl_3$@DPAHA. For pristine $CsPbCl_3$, the C 1s spectrum displayed peaks at 285.6 eV, 286.5 eV, and 289.7 eV, corresponding to C-C, C-N, and C=O bonds, respectively. After encapsulation of DPAHA, the C 1s peaks shifted to 286.0 eV, 286.7 eV, and 290.0 eV. These shifts toward higher binding energy suggest electron density withdrawal due to interfacial interactions, likely involving

coordination or hydrogen bonding between the perovskite surface and the acrylate matrix. In the O 1s spectrum, $CsPbCl_3$ showed peaks at 531.0 eV, 532.0 eV, and 533.0 eV, corresponding to Pb-O, C=O, and C-O bonds, respectively. After polymer encapsulation, these peaks appeared at 532.0 eV, 533.7 eV, and 534.7 eV. The consistent shift to higher binding energies indicates reduced electron density on oxygen atoms, further supporting strong interfacial interactions. The presence of polar ester groups in the acrylate network likely enhances these effects by increasing local electronegativity near the surface. The Cs 3d spectra of pristine $CsPbCl_3$ NCs exhibited two prominent peaks at 724.44 eV ($3d_{5/2}$) and 738.39 eV ($3d_{3/2}$), corresponding to the spin-orbit doublet of Cs^+. After encapsulation with DPAHA, these peaks shifted to 725.16 eV and 739.12 eV, respectively. This shift of approximately +0.7 eV toward higher binding energy indicates a reduction in electron density around the Cs^+ ions, likely due to electrostatic interactions or partial coordination between surface Cs atoms and the electronegative oxygen-containing groups (e.g., carbonyl and ether) of the acrylate matrix. The spin-orbit splitting showed a negligible increase from 13.95 eV to 13.96 eV, suggesting minimal perturbation of the core-level spin-orbit coupling, consistent with the preservation of the Cs^+ oxidation state. However, the intensity ratio of the $3d_{3/2}$ to $3d_{5/2}$ components decreased from 1.24 to 1.17 upon encapsulation. This slight reduction may be attributed to changes in surface sensitivity or photoelectron attenuation caused by the polymer layer, which can differentially affect signal intensities due to altered escape depths or local dielectric environments. Also, the Pb 4f spectrum of $CsPbCl_3$ revealed peaks at 138.20 eV ($4f_{7/2}$) and 143.12 eV ($4f_{5/2}$), characteristic of Pb^{2+} in the perovskite lattice. In the $CsPbCl_3$@DPAHA, these peaks shifted to 138.90 eV and 143.82 eV, respectively, also reflecting an upward shift of approximately +0.7 eV. This shift indicates a modification of the local electronic environment around Pb^{2+}, likely due to surface passivation or weak coordination interactions with the acrylate framework, which withdraws electron density and stabilizes the oxidized state. The spin-orbit splitting remained constant at 4.92 eV for both samples, confirming that Pb maintains its divalent oxidation state post-encapsulation. The intensity ratio ($4f_{5/2}$:$4f_{7/2}$) also showed a slight increase from 1.23 to 1.24, which could stem from subtle changes in surface morphology or polymer-induced modulation of the photoelectron scattering cross-section. The Cl 2p spectra were also analyzed to evaluate the chemical environment of chlorine in both pristine and polymer-encapsulated $CsPbCl_3$ NCs. For the pristine $CsPbCl_3$ sample, two peaks were observed at 197.7 eV and 199.3 eV, corresponding to the Cl $2p_{3/2}$ and Cl $2p_{1/2}$ spin-orbit components, respectively. These are attributed to Pb-Cl and C-Cl bonding environments,

indicating the presence of Cl^- coordinated to Pb^{2+} within the perovskite lattice and minor surface chloride species, possibly from surface ligands or residual precursors. After encapsulation with DPAHA, the Cl 2p peaks shifted to 198.49 eV and 200.1 eV, assigned to Pb-Cl and C-Cl environments, respectively. The observed shift of approximately +0.8 eV suggests a reduction in electron density on chloride ions, likely due to electrostatic interactions or hydrogen bonding between the acrylate matrix and surface-exposed chloride species. Such interactions alter the local dielectric environment and lead to binding energy shifts, consistent with changes observed in the Cs and Pb regions.

The spin-orbit splitting increased slightly from 1.6 eV (pristine $CsPbCl_3$) to 1.61 eV (encapsulated sample), indicating negligible perturbation of Cl^- spin-orbit coupling upon encapsulation. The intensity ratio (Cl $2p_{1/2}$: Cl $2p_{3/2}$) increased from 1.42 to 1.48, which may result from attenuation effects caused by the polymer overlayer or variations in surface composition, where a portion of Cl may be less exposed due to encapsulation and interfacial reorganization.

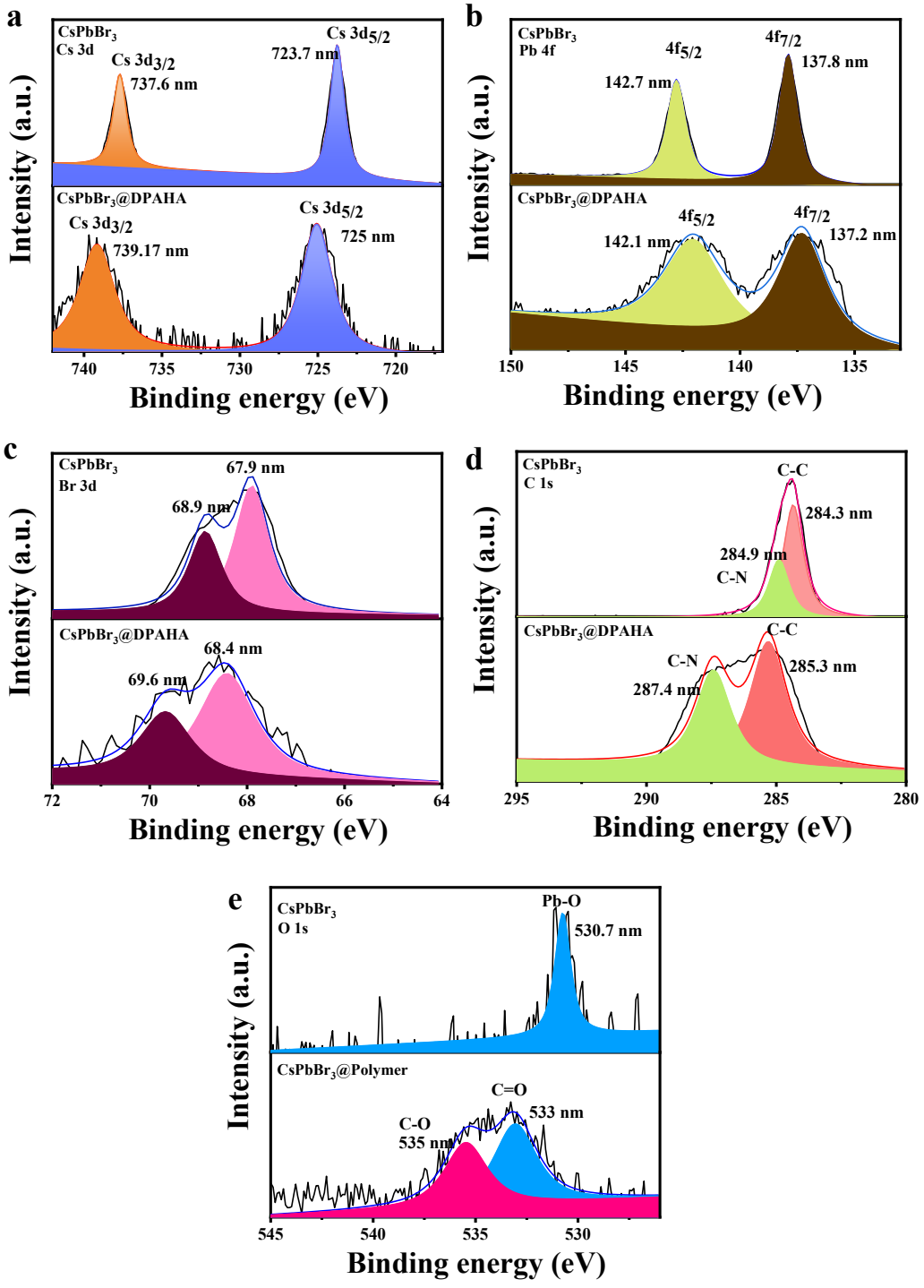

Fig. S12: **a.** XPS spectrum of Cs 3d of pure $CsPbBr_3$ and $CsPbBr_3$@DPAHA; **b.** XPS spectrum of Pb 4f of pure $CsPbBr_3$ and $CsPbBr_3$@DPAHA; **c.** XPS spectrum of Br 3d of pure $CsPbBr_3$ and $CsPbBr_3$@DPAHA; **d.** XPS spectrum of C 1s of pure $CsPbBr_3$ and $CsPbBr_3$@DPAHA; e. XPS spectrum of O 1s of pure $CsPbBr_3$ and $CsPbBr_3$@DPAHA.

XPS was again performed to investigate the surface chemical states of $CsPbBr_3$ NCs and $CsPbBr_3$@DPAHA, to evaluate the effects of polymer encapsulation on the electronic structure and surface composition in these materials. The C 1s spectrum of pristine $CsPbBr_3$ NCs exhibited peaks at 284.3 eV and 284.9 eV, arising from C-C and C-N bonds, respectively. These signals originate from surface organic residues or ligands remaining from synthesis. After encapsulation with DPAHA, the C 1s peaks appeared at 285.3 eV and 287.4 eV, indicating the presence of C–C and C=O bonds. The shift toward higher binding energies reflects a decrease in electron density around carbon atoms, likely due to electron-withdrawing effects from the acrylate matrix and the formation of interfacial interactions such as hydrogen bonding or dipole-dipole forces between surface species and polar carbonyl groups. In the O 1s region, the uncoated $CsPbBr_3$ sample showed a peak at 530.7 eV, related to Pb-O interactions, possibly from surface oxidation. In the encapsulated sample, peaks emerged at 533.0 eV and 535.0 eV, arising from C=O and C-O bonds present in the acrylate network. The appearance of these additional features, combined with a reduced contribution from Pb-O, indicates that the polymer effectively modifies the NC surface environment. These observations suggest a passivating effect, where the acrylate layer stabilizes the surface and mitigates further oxidation. The Cs 3d spectrum of $CsPbBr_3$ NCs exhibited peaks at 723.7 eV and 737.6 eV, corresponding to the $3d_{5/2}$ and $3d_{3/2}$ levels, respectively. In the $CsPbBr_3$@DPAHA, these peaks shifted to 725.0 eV and 739.17 eV, reflecting a positive shift of approximately 1.3–1.6 eV. This increase in binding energy indicates a reduction in electron density around the Cs^+ ions, suggesting interfacial interaction between the perovskite surface and the surrounding acrylate matrix. Such a shift is typically associated with partial coordination or electrostatic interaction with electron-withdrawing groups in the polymer. The spin-orbit splitting increased slightly from 13.9 eV to 14.1 eV, which may result from subtle changes in the local chemical environment. A noticeable decrease in the intensity ratio ($3d_{3/2}$: $3d_{5/2}$) from 1.17 to 1.04 further indicates changes in surface sensitivity, possibly due to attenuation or altered photoelectron escape depth caused by the encapsulating layer.

In the Pb 4f region, $CsPbBr_3$ displayed peaks at 137.8 eV and 142.7 eV for the $4f_{7/2}$ and $4f_{5/2}$ levels, respectively. After polymer encapsulation, the peaks were observed at 137.2 eV and 142.1 eV, indicating a slight negative shift of approximately 0.6 eV. This suggests a relatively more electron-rich environment around Pb^{2+} ions in the encapsulated system, possibly due to stabilization by nearby polymer functional groups that weakly interact with the Pb surface atoms. The spin-orbit splitting remained constant at 4.9 eV for both samples, consistent with

Pb^{2+} maintaining its oxidation state. The intensity ratio ($4f_{5/2}$:$4f_{7/2}$) was nearly unchanged, from 1.23 to 1.24, supporting the preservation of the Pb core-level structure despite surface modification. The Br 3d spectrum of pristine $CsPbBr_3$ NCs exhibited two peaks at 67.9 eV (Br $3d_{5/2}$) and 68.9 eV (Br $3d_{3/2}$), which reflect the presence of Br^- ions coordinated with Pb^{2+} within the perovskite lattice. These values are characteristic of bromide in a stable metal halide framework. In the $CsPbBr_3$@DPAHA, the Br 3d peaks appeared at 68.4 eV (Br $3d_{5/2}$) and 69.6 eV (Br $3d_{3/2}$), indicating a shift of approximately +0.5 to +0.7 eV. This shift to higher binding energy suggests a reduction in electron density around bromide ions, which may arise from interfacial interactions with the polymer matrix. Such changes typically occur when electronegative groups within the polymer alter the local dielectric environment or form weak electrostatic interactions near surface halide sites. The spin-orbit splitting increased slightly from 1.0 eV in the pristine $CsPbBr_3$ to 1.2 eV in the encapsulated composite, indicating a subtle change in the electronic environment surrounding the Br atoms, likely due to surface modification or slight structural rearrangement at the interface. The intensity ratio ($3d_{3/2}$: $3d_{5/2}$) decreased from 1.36 to 1.16, which may reflect attenuation of the photoelectron signal through the polymer overlayer or partial masking of surface Br sites by the acrylate matrix.

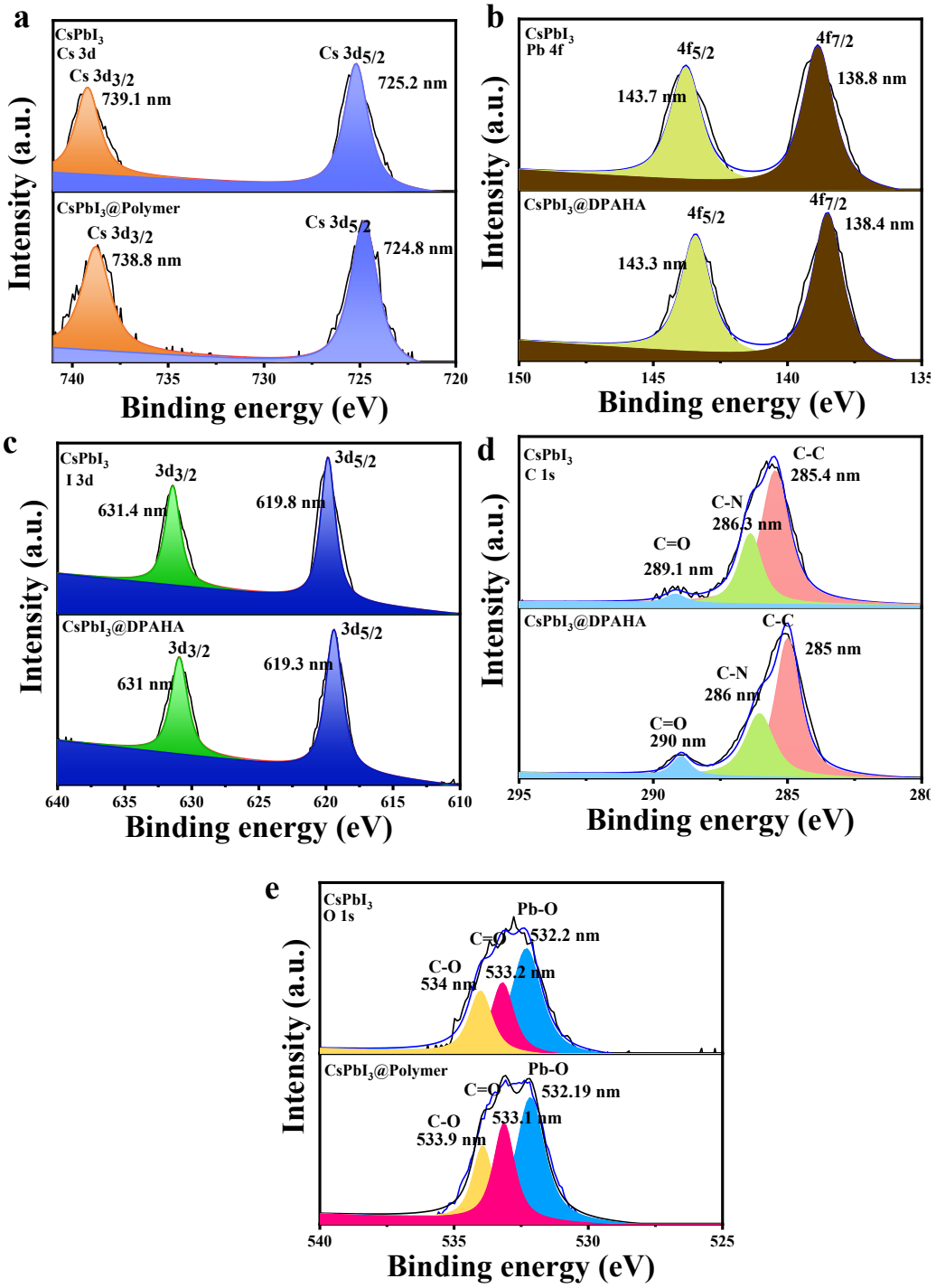

Fig. S13: **a.** XPS spectrum of Cs 3d of pure $CsPbI_3$ and $CsPbI_3$@DPAHA; **b.** XPS spectrum of Pb 4f of pure $CsPbI_3$ and $CsPbI_3$@DPAHA; **c.** XPS spectrum of I 3d of pure $CsPbI_3$ and $CsPbI_3$@DPAHA; **d.** XPS spectrum of C 1s of pure $CsPbI_3$ and $CsPbI_3$@DPAHA; e. XPS spectrum of O 1s of pure $CsPbI_3$ and $CsPbI_3$@DPAHA.

XPS was again performed to investigate the surface chemical states of $CsPbI_3$ NCs and $CsPbI_3$@DPAHA, to evaluate the effects of polymer encapsulation on the electronic structure and surface composition in these materials. The C 1s spectrum of pristine $CsPbI_3$ NCs exhibited three distinct peaks at 285.4 eV, 286.3 eV, and 289.1 eV, originating from C-C, C-N, and C=O bonding environments, respectively. These features are attributed to surface-bound organic residues, ligands, or unreacted precursors present on the NC surface. Upon encapsulation with DPAHA, the C 1s peaks were observed at 285.0 eV, 286.0 eV, and 290.0 eV, reflecting a subtle shift toward higher binding energy for the carbonyl species. This shift suggests electronic reorganization at the interface, likely resulting from interactions between polar acrylate groups and surface atoms on the perovskite NCs. Such interactions reduce the local electron density around the carbon atoms, particularly in oxygenated functionalities, indicating the formation of new interfacial bonding motifs or partial charge redistribution. In the O 1s spectrum, the spectrum of uncoated $CsPbI_3$ showed peaks at 532.2 eV, 533.2 eV, and 534.0 eV, attributed to Pb-O, C=O, and C-O bonds, respectively. These may result from partial surface oxidation and the presence of organic capping agents. In the $CsPbI_3$@DPAHA, similar peaks were detected at 532.19 eV, 533.1 eV, and 533.9 eV, maintaining the same trend but with slightly narrowed peak separation and reduced intensity for Pb-O. This indicates successful encapsulation and surface passivation, which likely reduces oxidation and stabilizes the nanocrystal surface through strong physical or chemical interactions with the acrylate framework. The consistent presence of carbonyl and ether-related oxygen peaks further confirms the incorporation of the DPAHA network around the perovskite core. The Cs 3d spectrum of pristine $CsPbI_3$ displayed two distinct peaks at 739.1 eV ($3d_{3/2}$) and 725.2 eV ($3d_{5/2}$), corresponding to the spin-orbit split components of Cs^+. In the $CsPbI_3$@DPAHA, these peaks were slightly shifted to 738.8 eV and 724.8 eV, respectively. The spin-orbit splitting values for the pristine and encapsulated materials were 13.9 eV and 14.0 eV, respectively, remaining nearly constant. This minor shift toward lower binding energy in the encapsulated sample indicates a reduction in the electrostatic interaction between Cs^+ ions and their surrounding electronic environment, possibly due to screening or passivation effects provided by the polymer matrix. Additionally, the intensity ratio ($3d_{3/2}$: $3d_{5/2}$) slightly decreased from 1.09 to 1.05, suggesting a change in surface stoichiometry or altered photoelectron attenuation due to polymer coverage. The I 3d core-level spectra of both pristine $CsPbI_3$ and $CsPbI_3$@DPAHA were examined to investigate the iodine chemical environment. For pristine $CsPbI_3$, the peaks appeared at 631.4 eV ($3d_{3/2}$) and 619.8 eV ($3d_{5/2}$), characteristic of iodide ions (I^-) coordinated within the perovskite lattice

as Pb-I bonds. In the encapsulated $CsPbI_3$@DPAHA sample, these peaks were observed at 631.0 eV and 619.3 eV, indicating a slight shift toward lower binding energies. This downshift implies a modest increase in electron density around iodine atoms, which can be attributed to weakened surface bonding or charge redistribution at the perovskite-polymer interface due to encapsulation. The spin-orbit splitting values were 11.6 eV and 11.7 eV for the pristine and encapsulated samples, respectively, showing negligible variation and suggesting that the I^- oxidation state and core-level splitting remain unaffected by the polymer network. However, the intensity ratio ($3d_{3/2}$: $3d_{5/2}$) slightly decreased from 1.18 in $CsPbI_3$ to 1.13 in $CsPbI_3$@DPAHA. This reduction may result from surface attenuation effects or partial surface shielding by the polymer matrix, which can affect the relative photoelectron escape depths from iodine atoms differently depending on their depth and local environment.

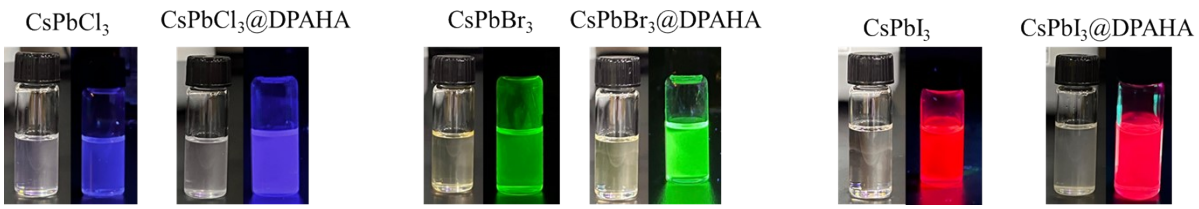

Fig. S14. Photographs of $CsPbX_3$ (X = Cl, Br, I) nanocrystal solutions before and after DPAHA modification under ambient light (left) and UV illumination (right). Pristine nanocrystals (left vial in each pair) show their characteristic emission, while DPAHA-modified samples (right vial in each pair) display enhanced and uniform luminescence, demonstrating the effect of surface passivation on optical properties.

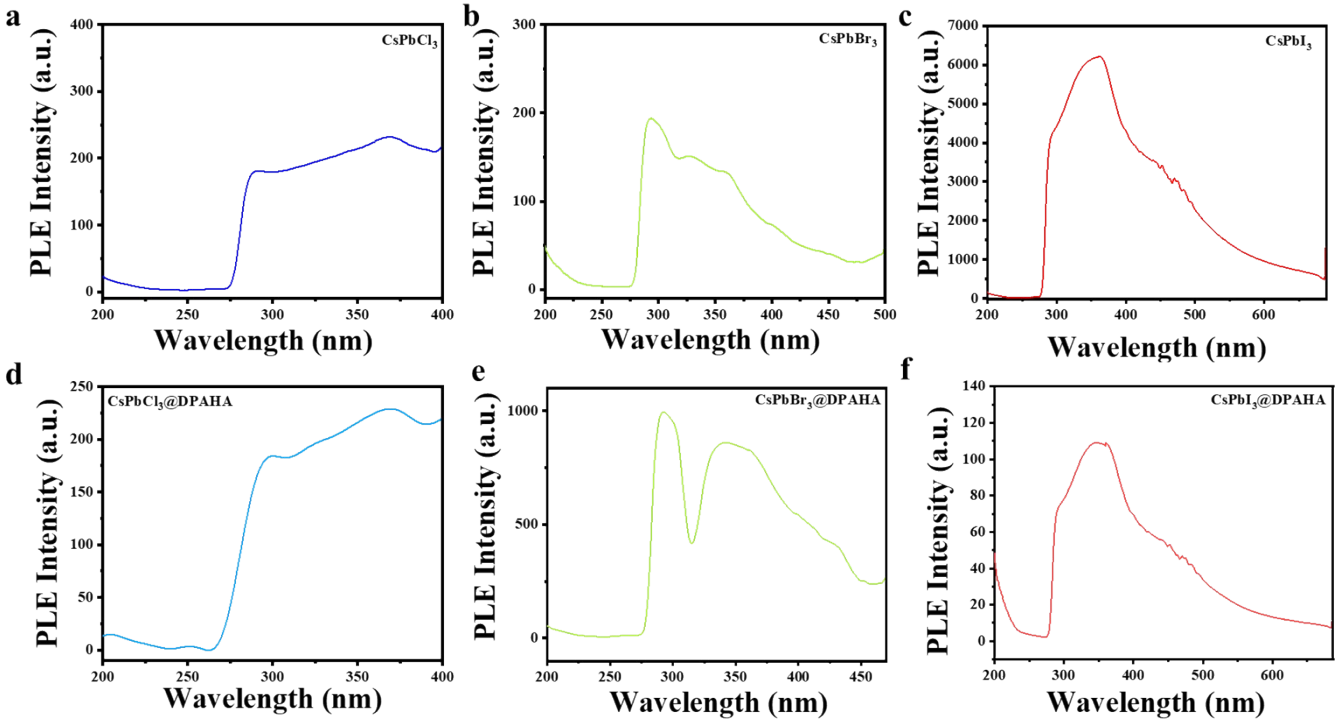

Fig. S15: **a.** PLE spectrum of $CsPbCl_3$; **b.** PLE spectrum of $CsPbBr_3$; **c.** PLE spectrum of $CsPbI_3$; **d.** PLE spectrum of $CsPbCl_3$@DPAHA; **e.** PLE spectrum of $CsPbBr_3$@DPAHA; **f.** PLE spectrum of $CsPbI_3$@DPAHA.

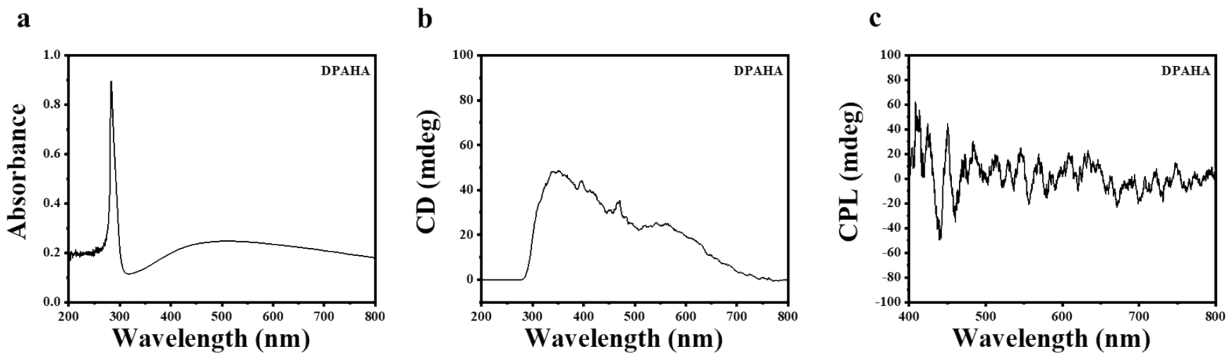

Fig. S16: Optical properties of DPAHA. (a) Absorbance, (b) CD, and (c) CPL.

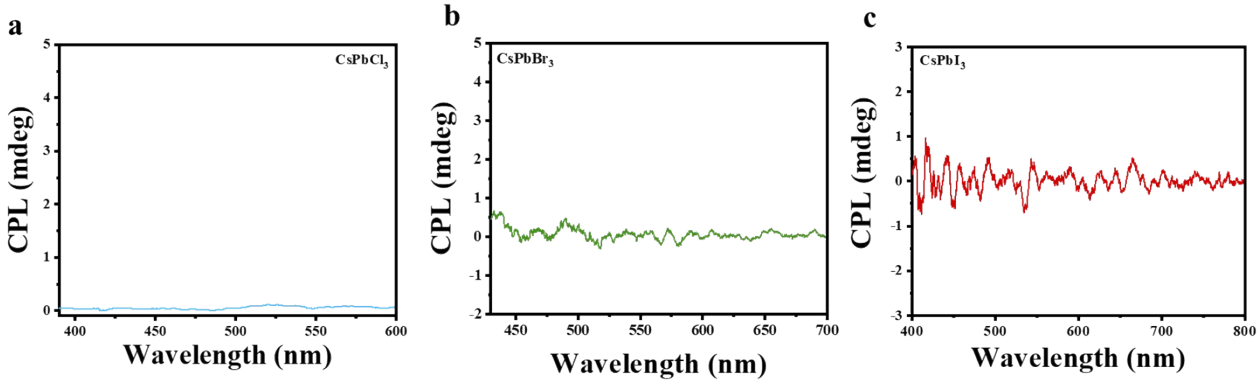

Fig. S17: **a.** CPL spectrum of pure $CsPbCl_3$; **b.** CPL spectrum of pure $CsPbBr_3$; **c.** CPL spectrum of pure $CsPbI_3$; **d.** g_{lum} spectrum of $CsPbCl_3$; **e.** g_{lum} spectrum of $CsPbBr_3$; **f.** g_{lum} spectrum of $CsPbI_3$.

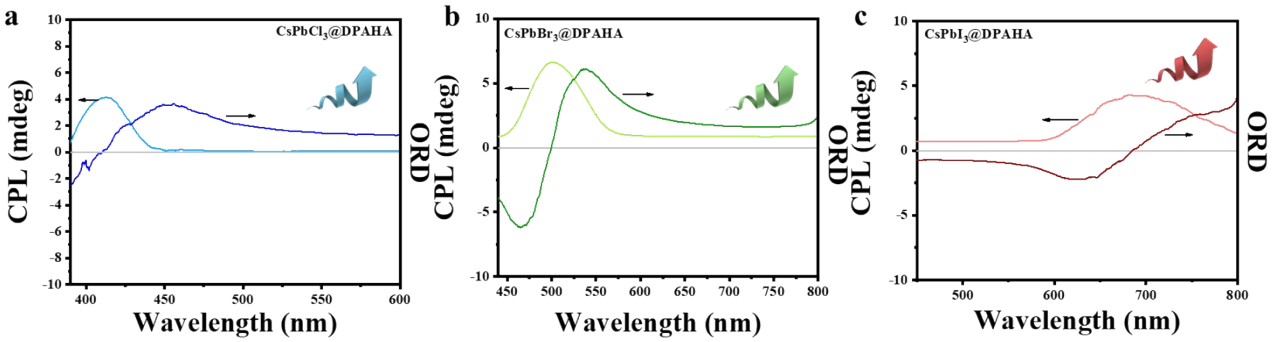

Fig. S18. CPL-ORD relationship of $CsPbX_3$ NCs within DPAHA matrix. a) $CsPbCl_3$@DPAHA, b) $CsPbBr_3$@DPAHA and c) $CsPbI_3$@DPAHA.

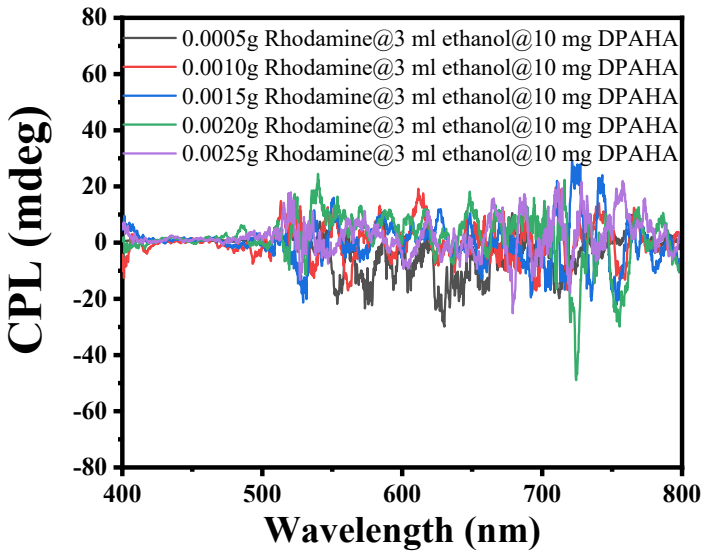

Fig. S19. CPL spectra of rhodamine B-DPAHA composite in ethanol.

Table S1. Comparison table for stability and CPL activity of photopolymerized polymer-perovskite composite

Perovskite	Polymer	Stability	CPL activity	Ref
$CsPbX_3$	QD-SH	≈100% PL retention after 260 days	⊗	1
$CsPbBr_3/MAPbBr_3$	polystyrene-b poly(2-vinylpyridine) (PS-b-P2VP) BCP	4 months	⊗	2
$MAPbBr_3$	lead bromide complexes	Not specified	⊗	3
$CsPbBr_3$	NKE-12	Several Days (Not specified)	⊗	4
$CsPbBr_3$	PMA	7 days	⊗	5
$MAPbBr_3$	MHP–styrene droplets	21 days	⊗	6
$CsPbX_3$	organosilicon polymer elastomer PDSP using PDMS-SH and D_4Vi	6 months	⊗	7
$CsPbX_3$	3-(trimethoxysilyl) propyl methacrylate	8h under UV, 6h in water	⊗	8
$CsPbBr_3$	TFE-HF	1 month	⊗	9
$CsPbBr_3$	Trithiocarbonate	100% retention after 7 days	⊗	10
$CsPbX_3$	DPAHA	More than 6 months	☑	(This work)

Table S2. Water contact angle (WCA) of pristine and $CsPbX_3$ @DPAHA-capped NCs

$CsPbCl_3$	**$CsPbCl_3$@DPAHA**	**Contact angle difference**
34.6°	98.0°	63.4°
$CsPbBr_3$	**$CsPbBr_3$@DPAHA**	**Contact angle difference**
65.7°	95.6°	29.9°
$CsPbI_3$	**$CsPbI_3$@DPAHA**	**Contact angle difference**
54.6°	116.6°	62°

References

1 Y. Tang, X. Zhang, K. Liao, L. Qiu, N. Du, L. Xiao, J. Ma, B. Wu, Z. Wu and G. Wang, *Adv. Opt. Mater.*, 2025, **13**, 1–10.

2 P. Ganswindt, I. Tepfenhart, A. Singldinger, A. Abfalterer, L. Spies, E. Kostyurina, M. Stadler, B. Nickel and A. S. Urban, *Adv. Opt. Mater.*, 2025, **13**, 11–15.

3 P. Zhang, G. Yang, F. Li, J. Shi and H. Zhong, *Nat. Commun.*, 2022, **13**, 6713.

4 M. Ahlawat, Neelakshi, R. Ramapanicker and V. Govind Rao, *ACS Appl. Mater. Interfaces*, 2024, **16**, 623–632.

5 X. Jin, K. Ma, J. Chakkamalayath, J. Morsby and H. Gao, *ACS Energy Lett.*, 2022, **7**, 610–616.

6 K. H. Kim, J. K. Park, S. H. Im and B. J. Park, *Part. Part. Syst. Charact.*, 2021, **38**, 1–7.

7 X. Jia, T. Shi, Q. Zhang, H. Huang, P. K. Chu, X.-F. Yu and R. He, *Chem. Eng. J.*, 2024, **500**, 156756.

8 X. Yang, C. Valenzuela, X. Zhang, Y. Chen, Y. Yang, L. Wang and W. Feng, *Matter*, 2023, **6**, 1278–1294.

9 Y. Liu, T. Chen, Z. Jin, M. Li, D. Zhang, L. Duan, Z. Zhao and C. Wang, *Nat. Commun.*, 2022, **13**, 1338.

10 X. Jin, K. Ma and H. Gao, *J. Am. Chem. Soc.*, 2022, **144**, 20411–20420.